

# Supplementary Materials for

# Combining tethered and untethered magnetic robots via a magnetically triggerable latch for target payload delivery and retrieval

Michael Brockdorff et al.

Corresponding author. Michael Brockdorff, <a href="mailto:elmbr@leeds.ac.uk">elmbr@leeds.ac.uk</a>, Pietro Valdastri</a>, <a href="mailto:p.valdastri@leeds.ac.uk">p.valdastri@leeds.ac.uk</a>

#### This PDF file includes:

Figs. S1 to S11
Tables S1 to S6
Legends for movies S1 to S6

Other Supplementary Materials for this manuscript include the following:

Movies S1 to S6

### **Supplementary Figures**

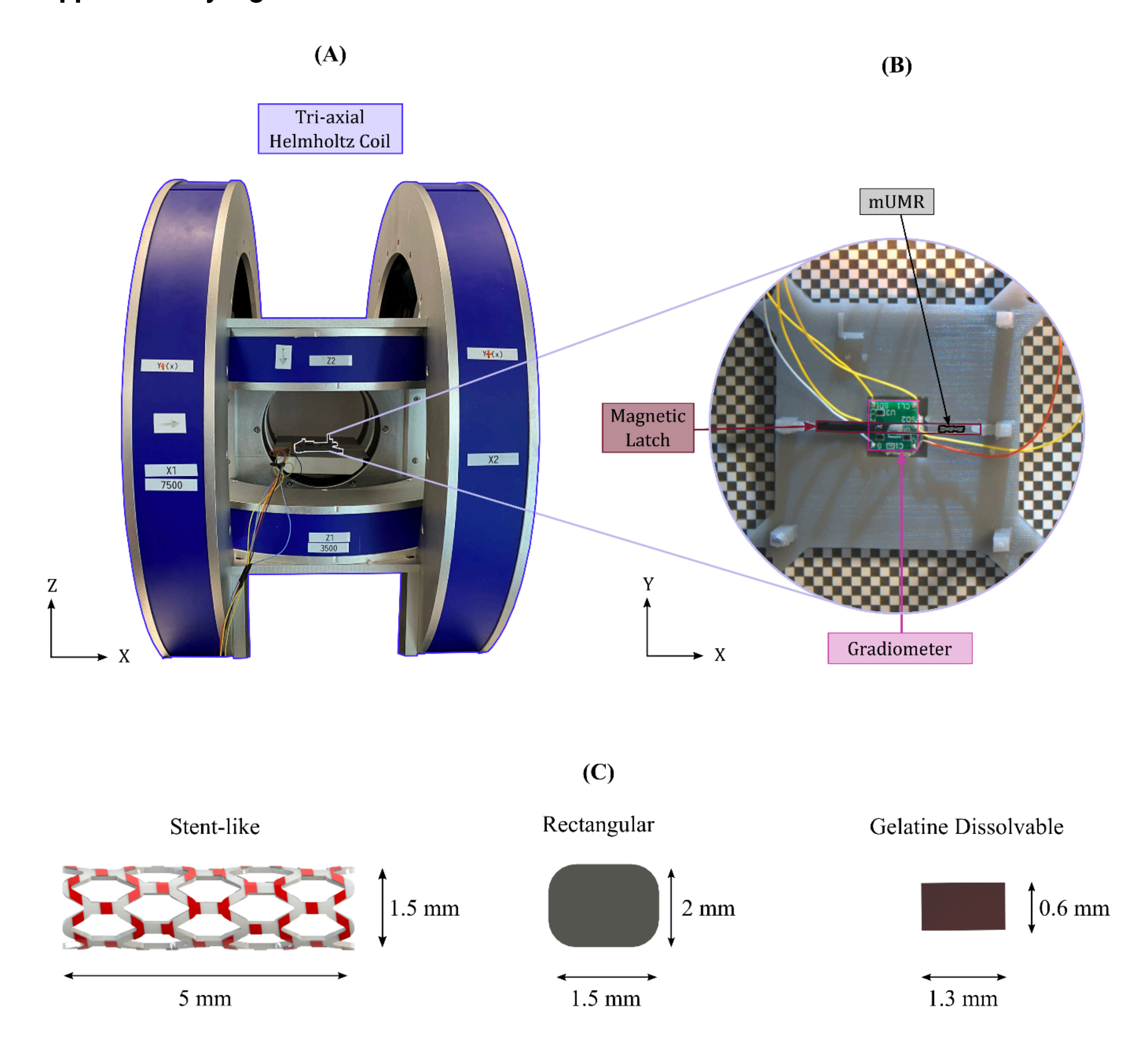


Fig. S1. Magnetic latch characterization setup. (A) The characterization rig was placed within a tri-axial Helmholtz coil system (3DXHC12.5-300, Dexing Magnet Tech. Co.Ltd, China), which provided up to 25 mT in three orthogonal directions. Each individual coil is paired with a bipolar DC power supply (DXKDP, Dexing Magnet Tech. Co. Ltd, China). (B) Magnetic latch characterization rig which includes a 3D printed mount to hold the magnetic latch and a magnetic gradiometer. (C) Schematic representation of the three mUMRs used including dimensions.

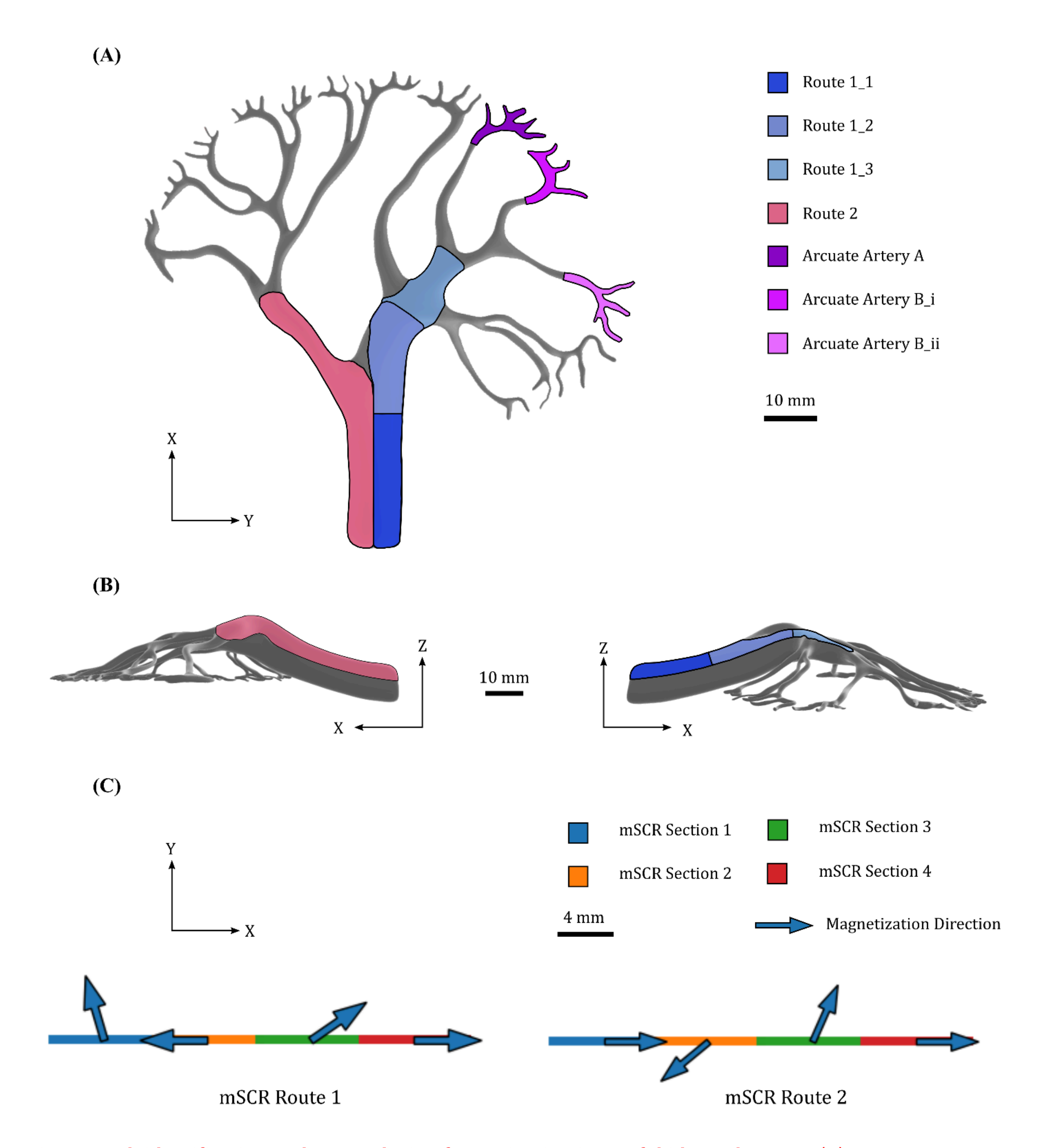


Fig. S2 Path identification and mSCR design for navigation in a soft kidney phantom. (A) 3D representation of the renal artery obtained by segmenting CTA data as seen from above. The routes for each navigation are highlighted in blue and pink for routes 1 and 2 respectively, with the arcuate arteries highlighted in shades of purple. (B) Model of the renal artery as seen from the side with intended routes highlighted. (C) Magnetic profiles of the two route specific mSCRs.

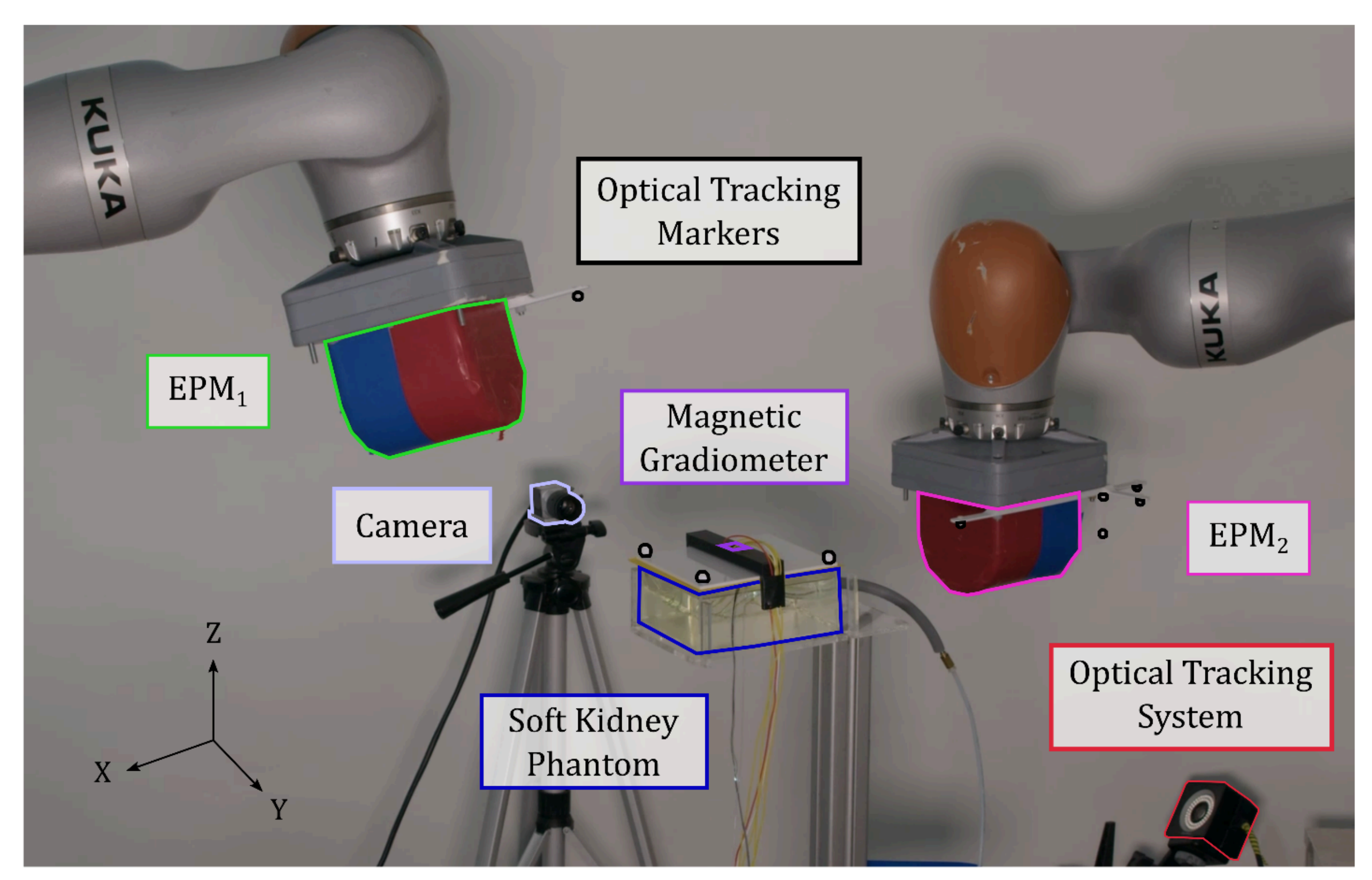


Fig. S3. dEPM platform used to control the navigation of the mSCR and mUMR within a soft kidney phantom.

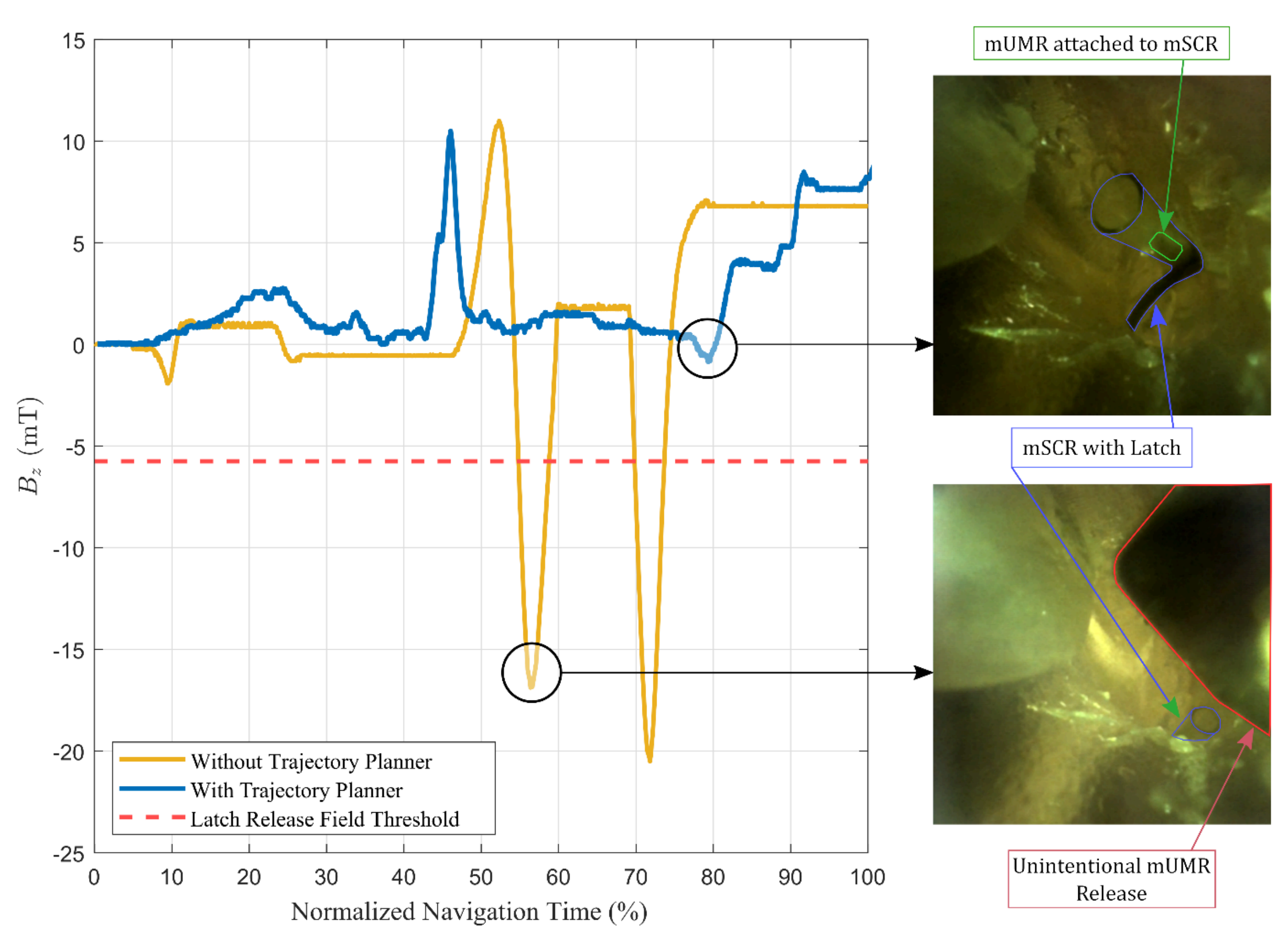
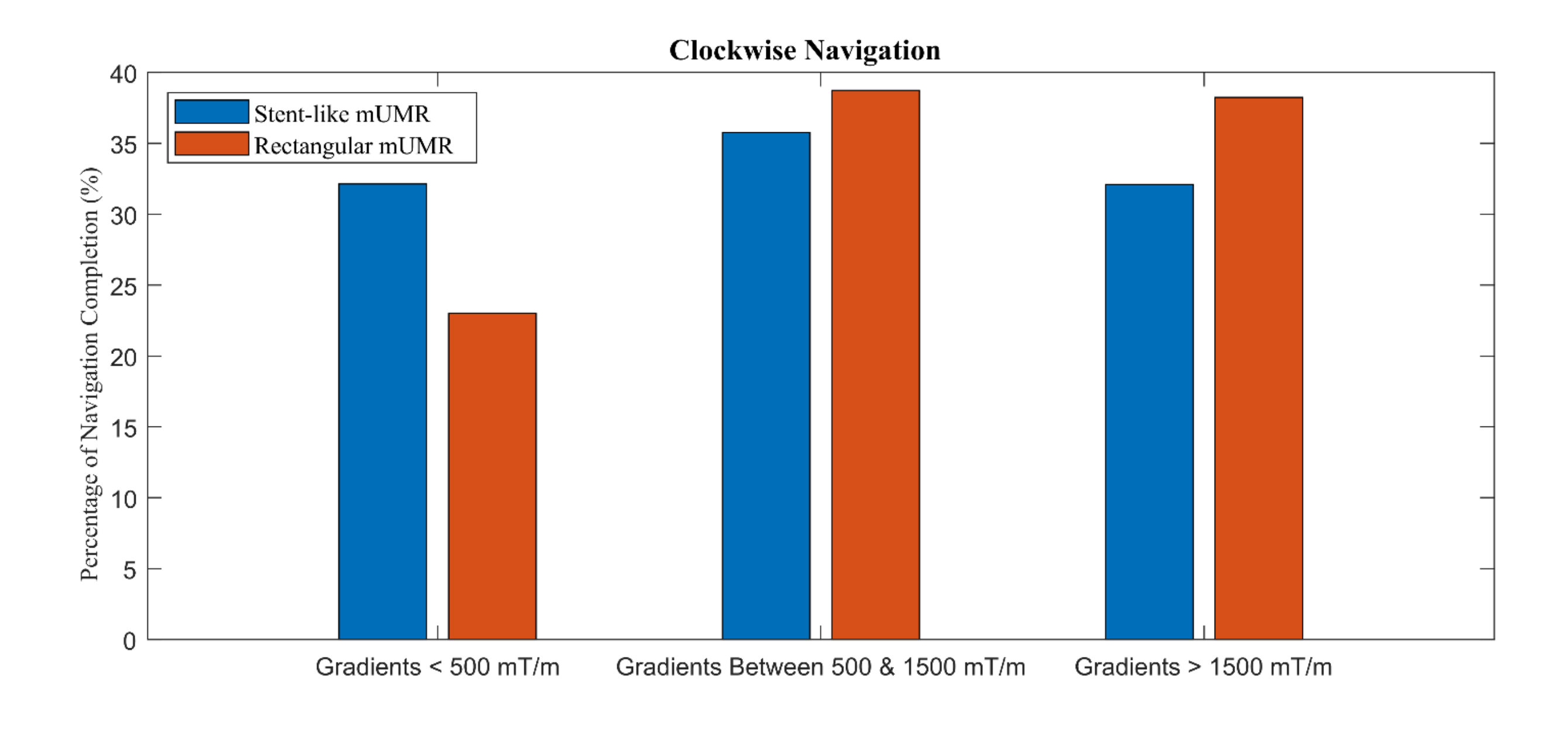


Fig. S4. Navigation in the soft kidney phantom route 1 with and without the hybrid trajectory planner. Without the hybrid trajectory planner, the field along the z-axis (which shares the axis of the release field for the magnetic latch) unintentionally exceeds the latch's release threshold, resulting in an unintended release of the mUMR. However, when using the hybrid trajectory planner, the release field is maintained at 15% of its required value, ensuring the navigation of the mSCR without releasing the mUMR. Once the navigation of the mSCR has been completed the mUMR is released and navigated independently.



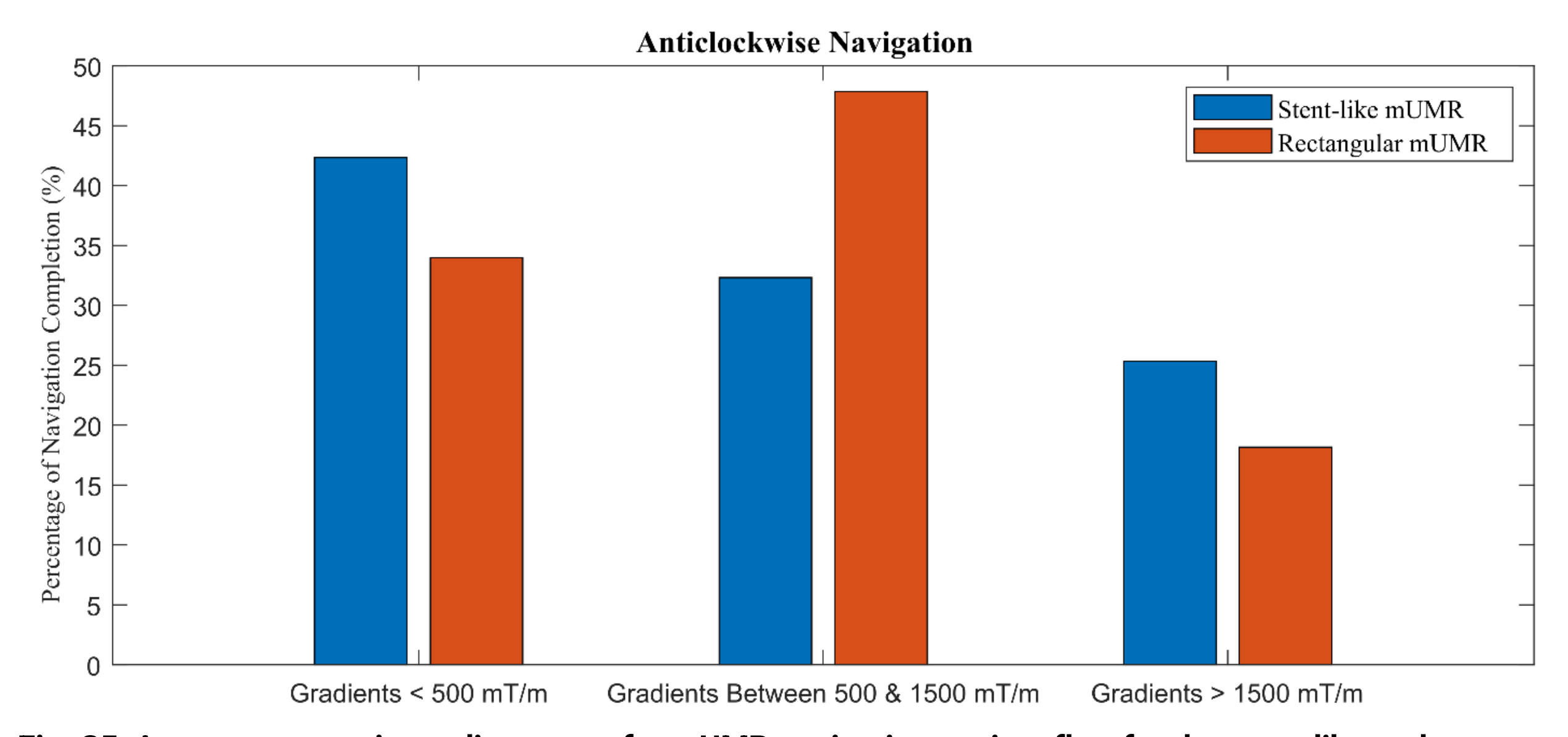
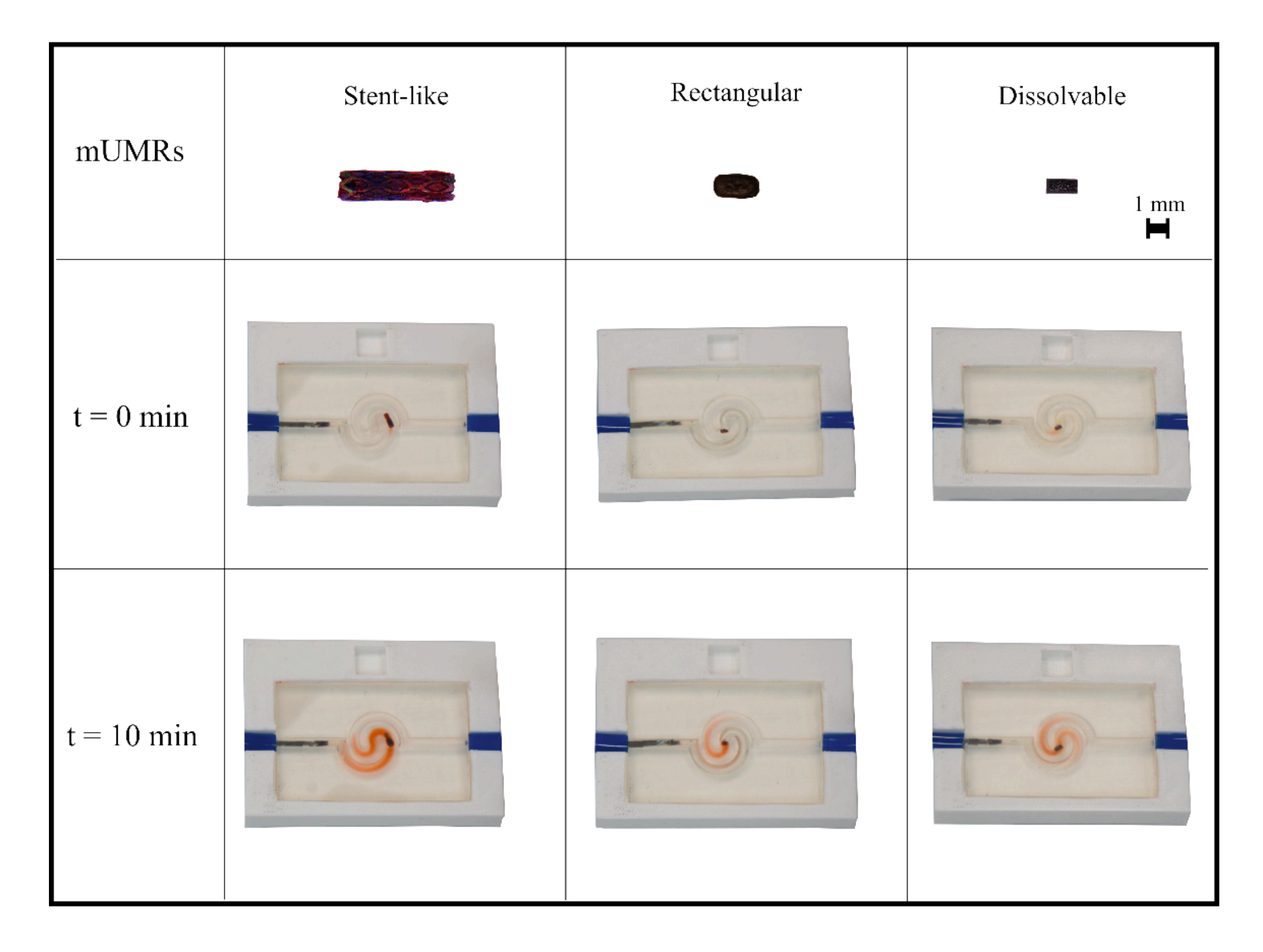


Fig. S5. Average magnetic gradient norm for mUMR navigation against flow for the stent-like and rectangular mUMRs.

**(A)** 



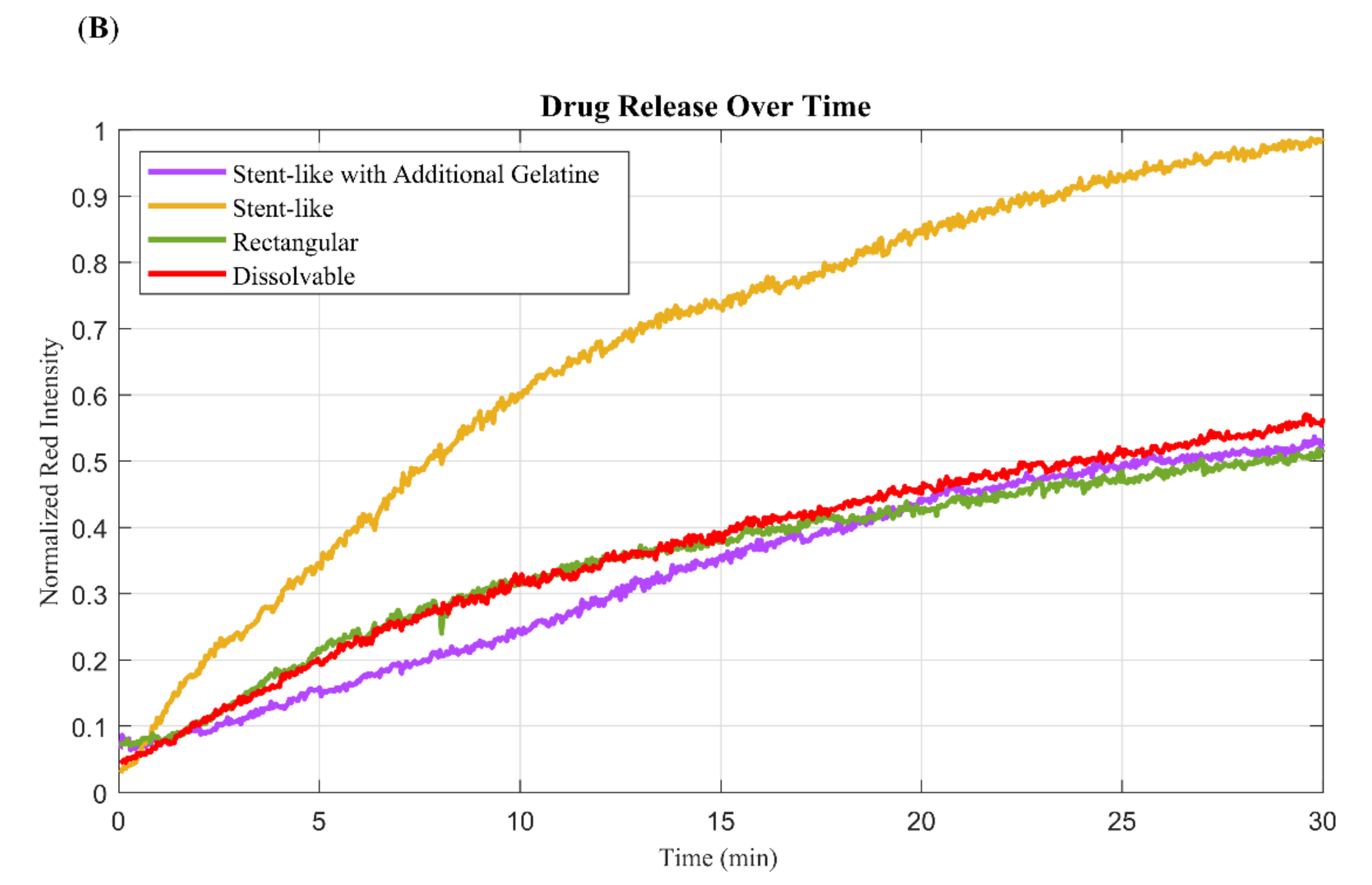
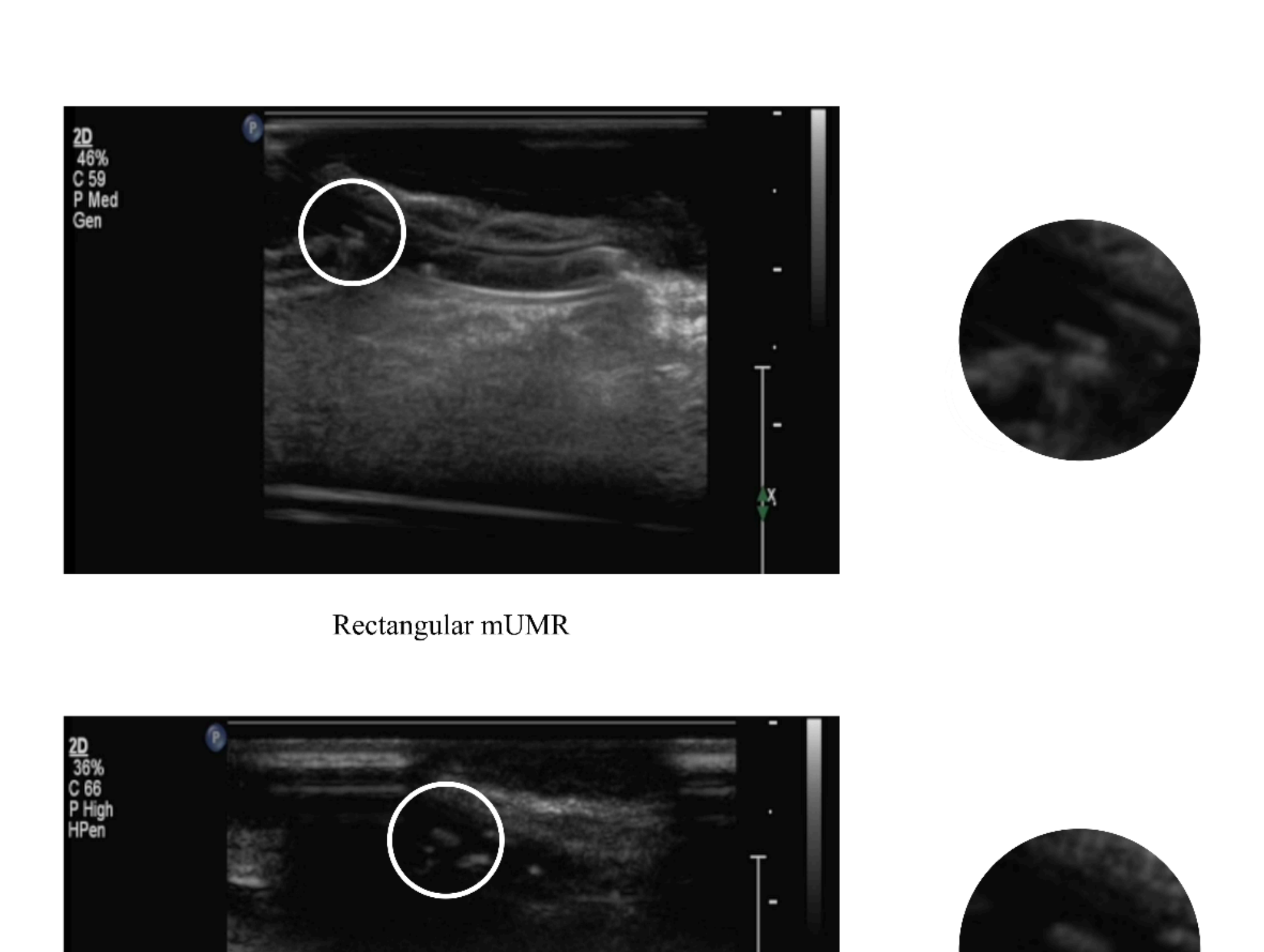
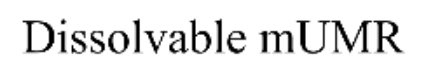
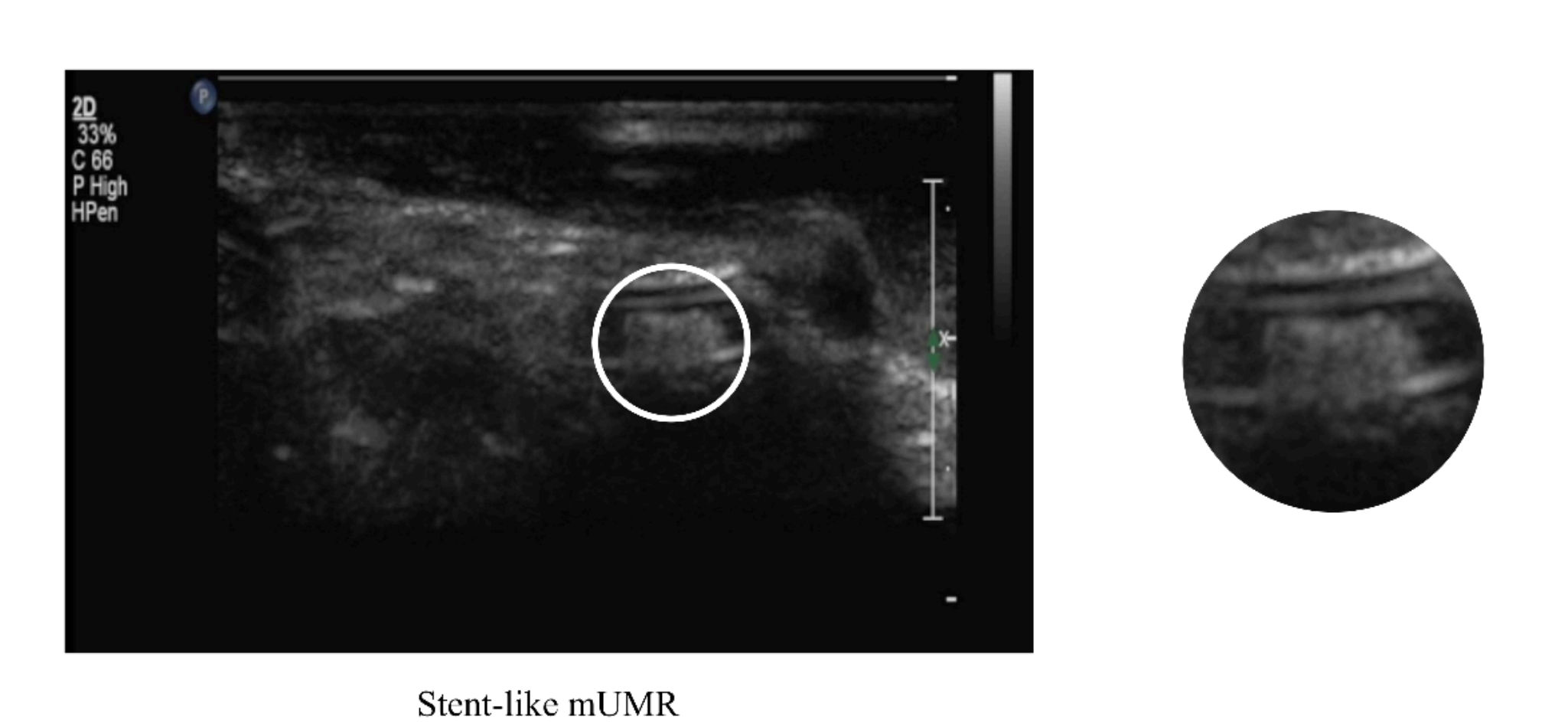


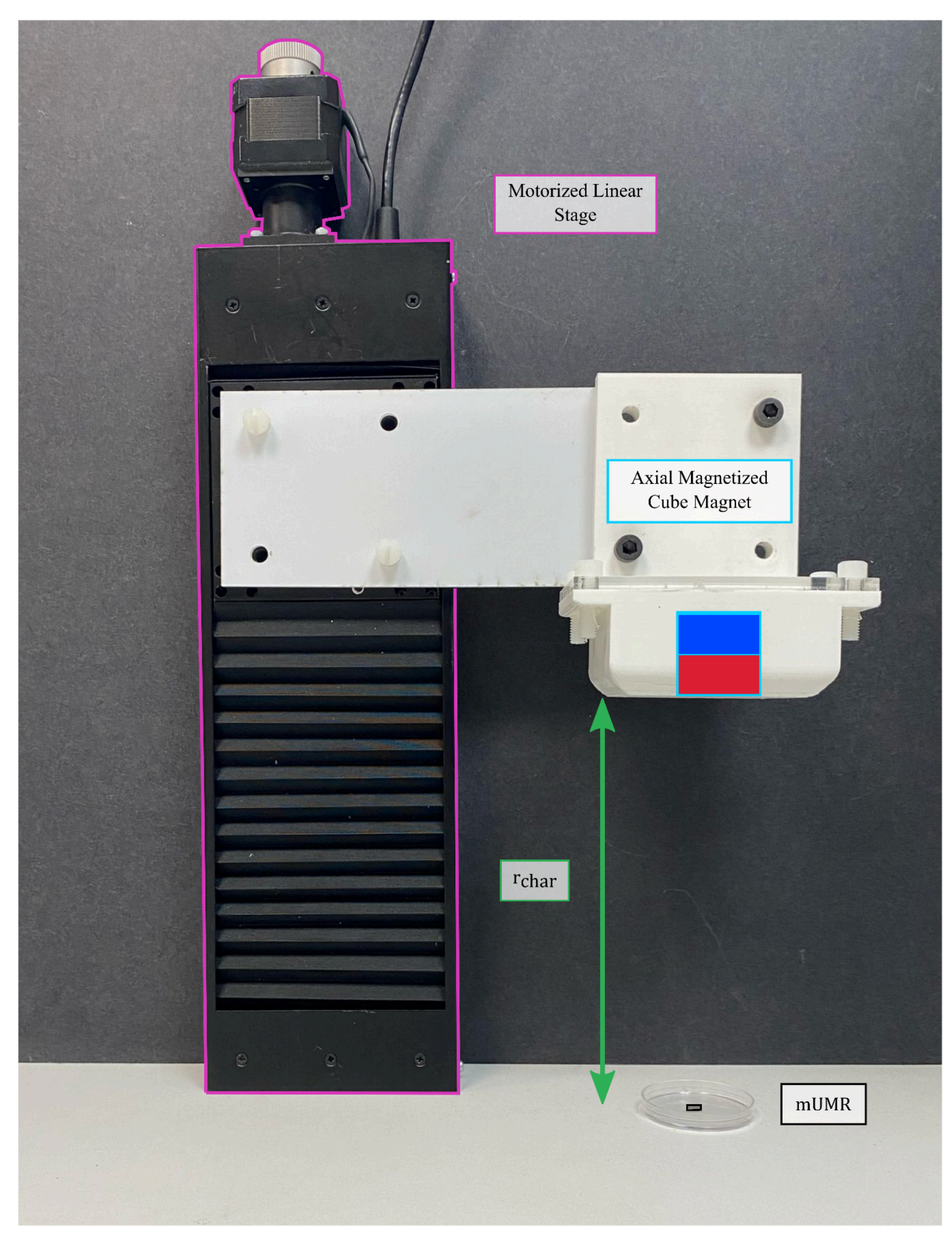
Fig. S6. Mock drug release over time for different mUMRs. (A) mUMRs coated with a mixture of red dye and gelatin, used to represent how the mUMRs could be coated with a drug. Snapshots showing the release of the mock drug into the phantom as time passes. (B) Graph comparing the release of mock drug between the different payloads over 30 min. The efficiency of drug release was calculated by measuring the ratio of red intensity in the red channel values relative to the number of red pixels in each video frame.



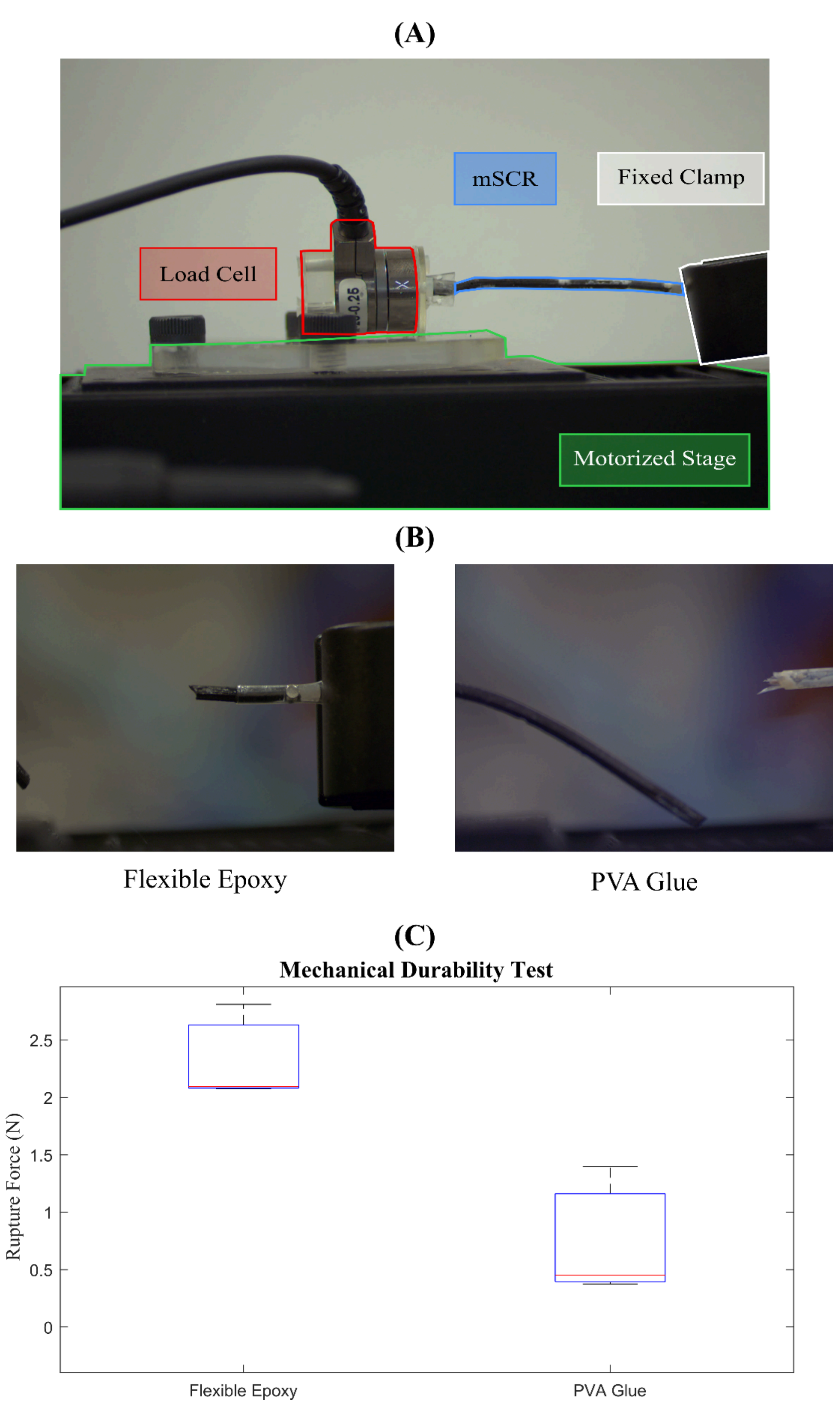




**Fig. S7. Visibility of mUMRs under ultrasound.** Comparison of the visibility of various classes of mUMRs within the vasculature of an *ex vivo* porcine kidney as seen under ultrasound. The stent-like mUMR demonstrates the clearest visibility. The clarity of other mUMRs can be enhanced by incorporating

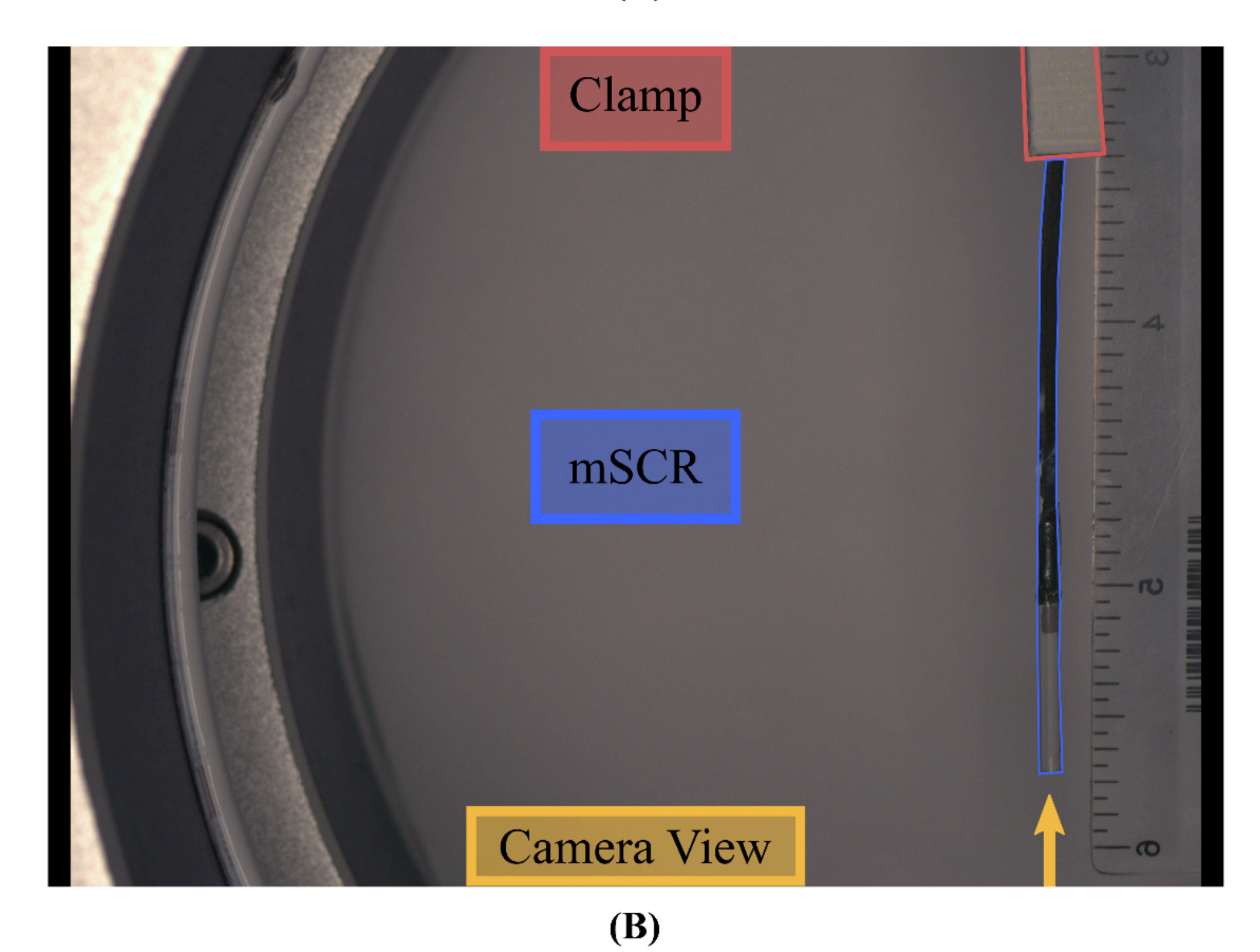


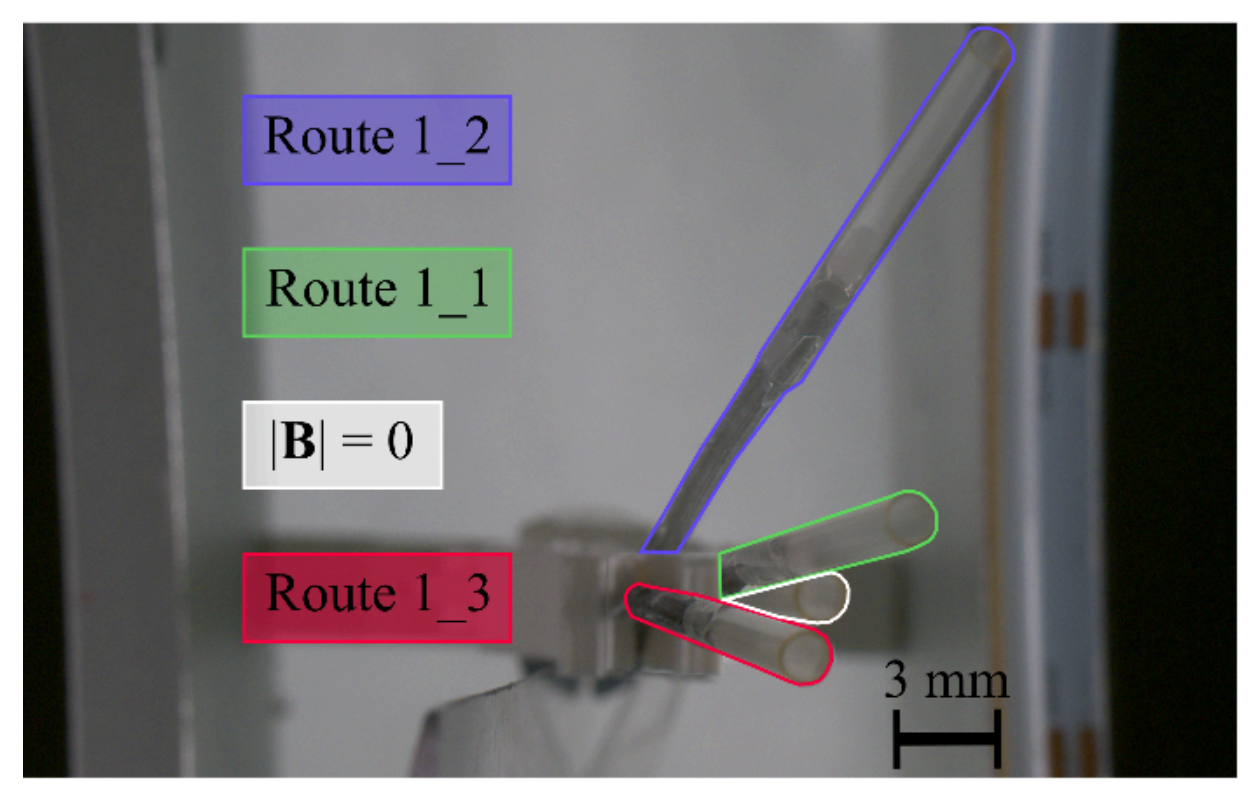
**Fig. S8. mUMR magnetic moment characterization setup.** A linear motorized stage was used to lower an axial magnetized cube magnet towards the mUMR. Once the magnetic force overcame the gravitational force on the mUMR, the distance  $\mathbf{r_{char}}$  was measured. This distance along with the mass of the mUMR was used to calculate its magnetic moment.



**Fig. S9: Mechanical durability test. (A)** Setup to test the mechanical durability of different adhesives used when attaching the magnetic latch to the mSCR. (**B**) Different points of failures where observed for the different adhesives. (**C**) Qualitative comparison of the different forces required to rupture the two types of

**(A)** 





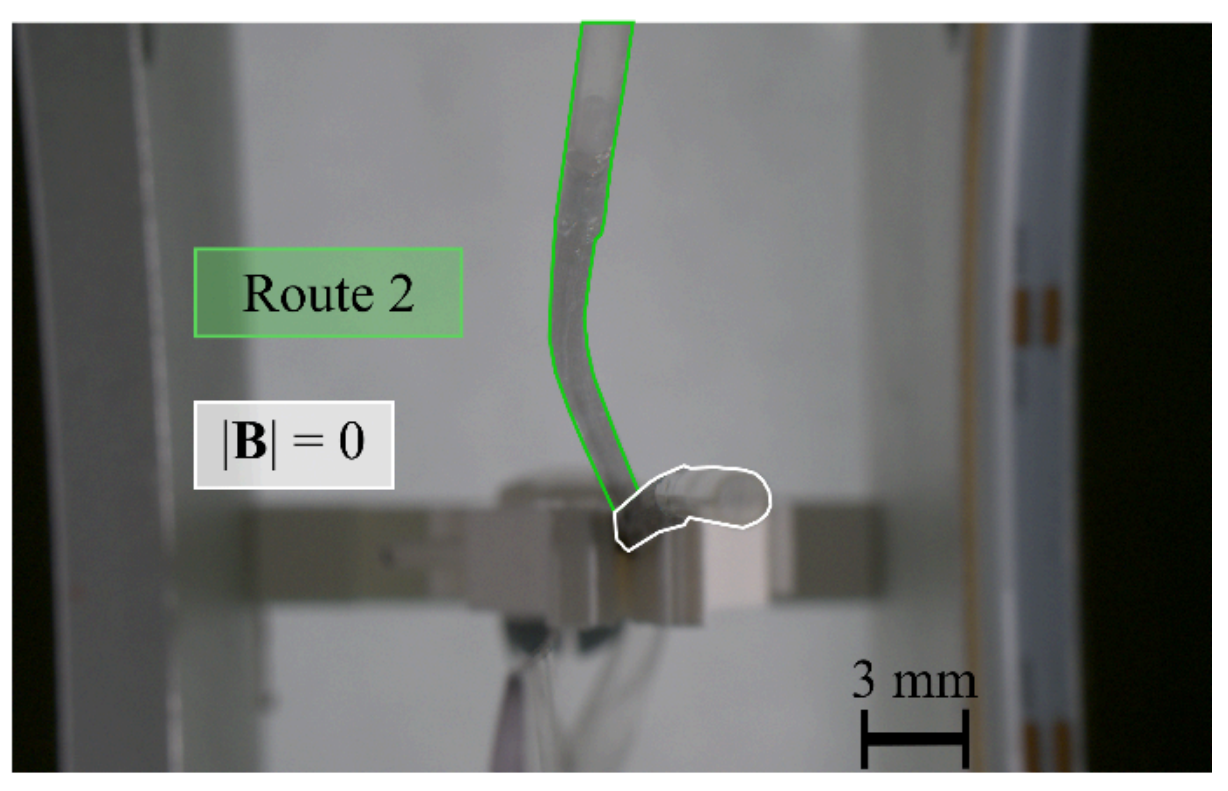


**Fig. S 10: Out-of-plane deformation characterization.** The latch magnet which lies orthogonal to the magnetization plane of the mSCRs, may cause some undesired out-of-plane deformation. (**A**) a tri-axial Helmholtz coil used to generate the required magnetic fields for each section of the navigation path for each mSCR. (**B**) The out-of-plane deformation was measured using a camera placed underneath the mSCRs.

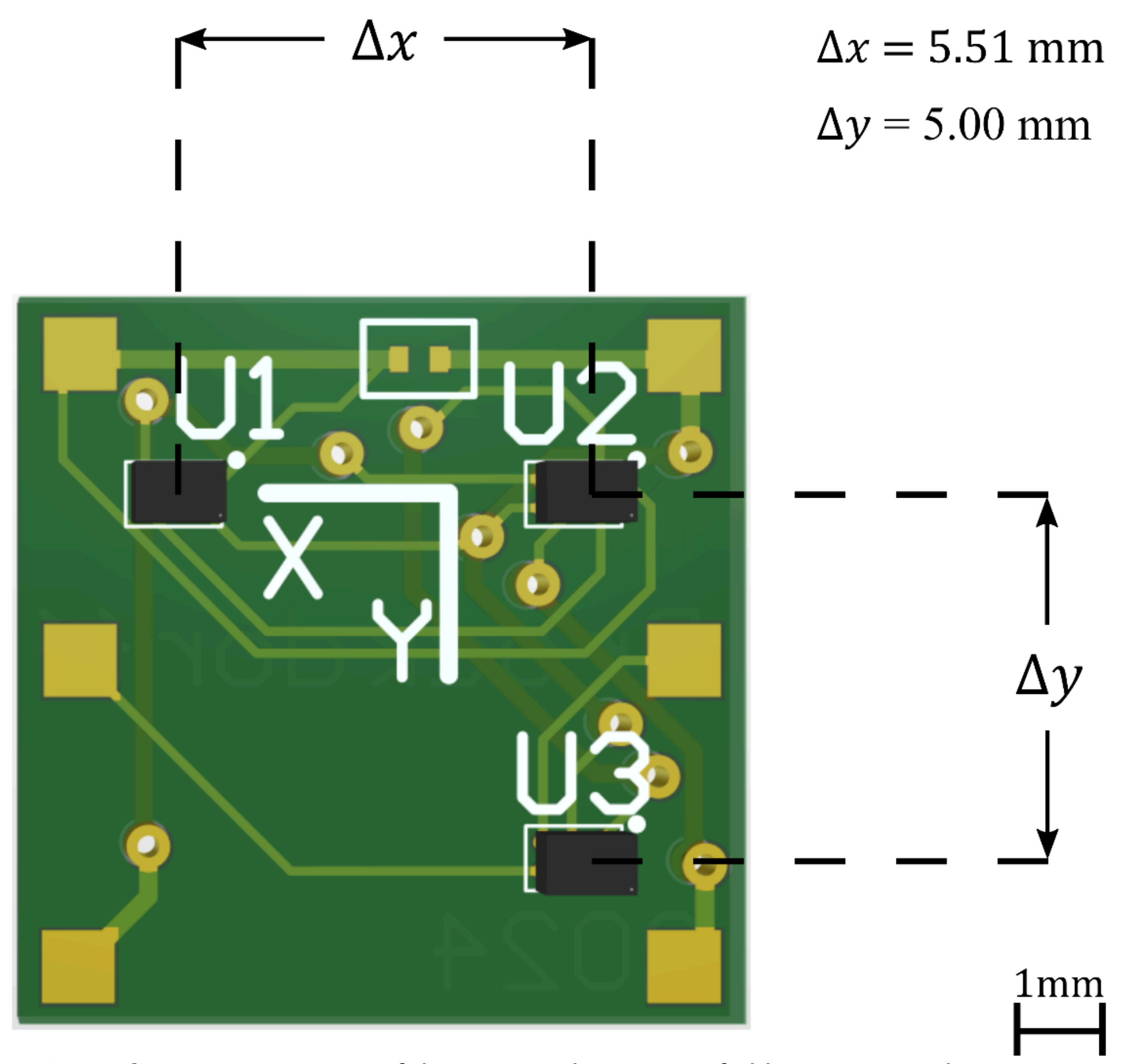


**Fig. S11. Magnetic Gradiometer.** Consists of three tri-axial magnetic field sensors used to approximate the magnetic field and gradient at the position of the sensor U2 using finite differences.

## **Supplementary Tables**

Table S1. Comparison of magnetic field required to release each type of mUMR from the magnetic latch with varying separation layer thicknesses.

Name of mUMR	Magnetic Moment (Am <sup>2</sup> )	Release Field (mT)		
		Separation Layer	Separation Layer	Separation Layer
		2.5 mm	4 mm	7.5 mm
Rectangular 1:0.75	$3.95 \times 10^{-5}$	$4.86 \pm 0.36$	$1.60 \pm 0.21$	$1.17 \pm 0.37$
Rectangular 1:1	$5.57 \times 10^{-5}$	$5.35 \pm 0.45$	$1.49 \pm 0.12$	$0.98 \pm 1.00$
Rectangular 1:1.5	$8.58 \times 10^{-5}$	$5.50 \pm 0.44$	$1.82 \pm 0.15$	$1.65 \pm 0.28$
Dissolvable	$4.41 \times 10^{-5}$	$10.04 \pm 0.85$	$2.91 \pm 0.16$	$0.94 \pm 0.19$
Stent-like	$1.27 \times 10^{-4}$	$2.50 \pm 0.67$	$2.01 \pm 0.94$	

Table S2: Estimated latching force for each class of mUMR at different separation layer thicknesses. The latching force was calculated using the approximation shown in (4).

Name of mUMR	Magnetic Moment (Am²)	Estimated Latching Force   f <sub>latch</sub>    (mN)			
		Separation Layer	Separation Layer	Separation Layer	
		2.5 mm	4 mm	7.5 mm	
Rectangular 1:0.75	$3.95 \times 10^{-5}$	0.149	0.036	0.004	
Rectangular 1:1	$5.57 \times 10^{-5}$	0.210	0.051	0.006	
Rectangular 1:1.5	$8.58 \times 10^{-5}$	0.324	0.078	0.009	
Dissolvable	$4.41 \times 10^{-5}$	0.254	0.053	0.006	
Stent-like	$1.27 \times 10^{-4}$	0.115	0.040		

Table S3: Characterization of the maximum out-of-plane deformation produced by the tip magnet, which actuates the latching system.

<b>Navigation Route</b>	Route 1_1	Route 1_2	Route 1_3	Route 2
Out-of-plane deformation	2.55	4.85	0.65	3.96
(mm)				

Table S4: Estimated torque needed to rotate each mUMR and hence, release it from the magnetic latch for different separation layer thicknesses. The torque was calculated using the dipole approximation for magnetic torque.

	Estimated Release Torque   τ   (mN.m <sup>-1</sup> )			
Name of mUMR	Separation Layer 2.5	Separation Layer 4	Separation Layer 7.5	
	mm	mm	mm	
Rectangular 1:0.75	0.1920	0.0632	0.0462	
Rectangular 1:1	0.2980	0.0830	0.0546	
Rectangular 1:1.5	0.4867	0.1611	0.1460	
Dissolvable	0.4428	0.1283	0.0415	
Stent-like	0.3175	0.2553		

Table S5. The magnetic field required to navigate each mSCR through their respective routes.

Navigation Route		Magnetic Field (mT)	
	Bx	Ву	Bz
Route 1_1	0.5	-3.0	1.0
Route 1_2	15.0	0	1.75
Route 1_3	3.5	3.0	7.25
Route 2	12.5	-0.5	-5

Table S6. Average navigation times for the stent-like and rectangular mUMRs in the vascular phantom. The mUMRs were navigated into two directions, clockwise and counterclockwise. Re-attachment to the latch was always done against flow.

	Clockwise		Counterclockwise	
	Stent-like	Rectangular	Stent-like	Rectangular
Release (min)	2.88 ± 0.98	2.03 ± 0.75	1.41 ± 1.34	0.75 ± 0.92
Navigation (min)	11.84 ± 6.30	5.37 ± 5.65	5.60 ± 6.06	4.42 ± 2.37
Re-attachment (min)	8.26 ± 1.11	10.39 ± 10.07	7.71 ± 9.30	7.44 ± 2.31

#### **Supplementary Movies**

#### Movie S1. Magnetic latch characterization and release of different mUMRs.

This video demonstrates the characterization setup for the magnetic latch, showing the release of stent-like, rectangular, and dissolvable mUMRs.

#### Movie S2. mSCR navigation in a soft kidney phantom.

This video demonstrates the navigation of two mSCRs along different routes in a soft kidney phantom, using the hybrid trajectory planner. Without the planner, the mUMR is prematurely released from the magnetic latch before the mSCR reaches its final destination.

#### Movie S3. Influence of blood flow on mUMR navigation and retrieval.

This video demonstrates the navigation of rectangular and stent-like mUMRs both with and against flow at a rate of 1.3 L/min. It also shows how mUMRs can reattach to the magnetic latch against the flow. Additionally, the effect of insufficient magnetic coupling between the mUMR and EPM is demonstrated.

#### Movie S4. Delivery and retrieval of a stent-like mUMR under ultrasound guidance.

This video demonstrates the ultrasound-guided release and reattachment of a stent-like mUMR in a porcine kidney model. The impact of insufficient magnetic coupling between the mUMR and EPM is also shown.

#### Movie S5. Integrated mSCR navigation with mUMR deployment and retrieval.

This video shows the navigation of an mSCR with an integrated magnetic latch with a clear, 3D printed, kidney phantom. Once successfully progressing through route 1 of the phantom, the mUMR is released from the magnetic latch and independently navigated to the arcuate arteries. Once navigation is complete the mUMR is navigated back to the mSCR were it reattaches to the magnetic latch and is removed from the anatomy.

#### Movie S6. Magnetic latch mechanical durability tests.

This video demonstrates the durability of the magnetic latch, showcasing the difference when using a flexible epoxy compared to PVA glue as a magnetic latch bonding agent.